Sensors & Transducers, Vol. 207, Issue 12, December 2016, pp. 21-29

www.sensorsportal.com

Sensors & Transducers

Published by IFSA Publishing, S. L., 2016
http://www.sensorsportal.com

Ultra-fast Sensor for Single-photon Detection in a Wide Range of the Electromagnetic Spectrum

*** Astghik KUZANYAN, Armen KUZANYAN, Vahan NIKOGHOSYAN**
Institute for Physical Research NAS of Armenia, Ashtarak-2, Ashtarak, 0203, Republic of Armenia
* Tel.: +37410288150, fax: +34723231172
* E-mail: akuzanyan@yahoo.com

Received: 5 November 2016 /Accepted: 5 December 2016 /Published: 30 December 2016

Abstract: The results of computer simulation of heat distribution processes taking place after absorption of single photons of 1 eV-1 keV energy in three-layer sensor of the thermoelectric detector are being analyzed. Different geometries of the sensor with tungsten absorber, thermoelectric layer of cerium hexaboride and tungsten heat sink are considered. It is shown that by changing the sizes of the sensor layers it is possible to obtain transducers for registration of photons within the given spectral range with required energy resolution and count rate. It is concluded that, as compared to the single layer sensor, the thee-layer sensor has a number of advantages and demonstrate characteristics that make possible to consider the thermoelectric detector as a real alternative to superconducting single photon detectors.

Keywords: Thermoelectric, Single-photon detector, Multi-layer sensor.

1. Introduction

The increased interest in recent years to sources and detectors of single photons is due to remarkable progress in different areas of science and technology. Single photon detectors capable to determine the photon energy and to provide high count rates are demanded in quantum electronics, astrophysics, high energy physics, quantum informatics, telecommunication systems, quantum metrology, measuring systems for applications in medicine, homeland security and other fields [1-4]. A revolution in photon detection took place in connection with the development of detectors based on superconductivity [5-6]. These tools significantly improved the sensitivity of measurements across the electromagnetic spectrum, from radio waves through visible light to gamma rays. Superconducting Single-Photon Detectors (SSPD) come in two main types: thermal (TES) and pair-breaking (STJ). With both types, the energy of an individual photon (and hence its frequency) is revealed by the strength of the device's output signal. Among the developments of the last 15 years, superconducting nanowire single-photon detectors (SNSPD) are considered as the most promising [7]. In terms of characteristics they compare favorably all earlier known detectors, possess a low dark-count rate, gigahertz count rate and are able to register photons in a wide range of the electromagnetic spectrum [8-10]. The thermoelectric single-photon detector (TSPD) possesses very close characteristics. The physical concept of the TSPD has been suggested in 2000 [11-12] being the only new approach in single photon detection methods introduced during quite a long time period [13]. The next investigations have shown that TSPD may compete with SNSPD, since in some properties and characteristics they are better [14-19]. Computer simulation of heat distribution processes in a single layer sensor of TSPD has revealed a number of peculiarities of TSPD, in

particular the dependence of the response on the area of the photon thermalization in the absorber [20-23]. Recently, the idea of a three-layer TSPD sensor was proposed [24] providing for independence of the response on the thermalization region [25]. In the present work the results of computer simulation of the heat distribution processes in a three-layer sensor of the TSPD occurring after absorption of photons with energies from 1 eV to 1 keV are presented.

2. Detection Pixels of TSPD

The design, peculiarities and characteristics of the single layer TSPD sensor were investigated in [11-12, 26]. The sensor contains two absorbers made of a heavy metal which are deposited on a dielectric substrate and coupled to each other by a thermoelectric bridge (Fig. 1(a)). When a photon enters the absorber its temperature rises, in comparison to that of the second absorber, leading to appearance of a voltage; by measuring this voltage the fact of absorption can be registered and the energy of the photon determined. Operation of such a sensor does not require any additional power source or applied voltage and, hence, no additional contacts. The TSPD sensor has remarkably simple design and provides for possibility to create detector matrix consisting of assemblage of sensors with very simple electronic structure. Such a sensor has, however, deficiencies limiting its application. The photon energy is being determined taking integral of the signal timing dependence. If the time decay of the signal to the background value is higher than the time of heat propagation through the metal-dielectric boundary, the so called Kapitza boundary, then a part of the heat extracted by the photon will pass to the substrate making impossible to determine the photon energy. The photon energy cannot be determined by the maximal value of the arising signal, since the temporal behavior depends on the area of the photon thermalization. The three-layer design of the TPSD sensor (Fig. 1(b)) avoids such dependence and the possibility of heat draft from absorber to the substrate.

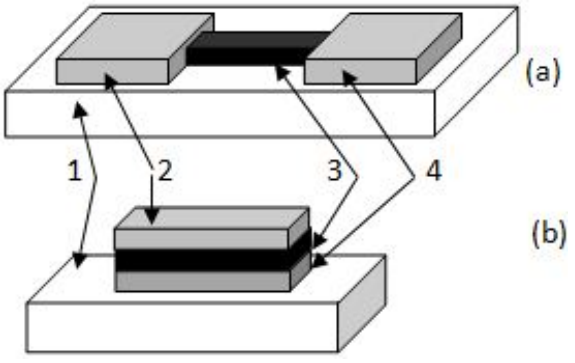

Fig. 1. Single layer (a), and three-layer (b) sensors design: 1 – substrate; 2 – absorber; 3 – thermoelectric layer; 4 – heat sink.

3. Computing Technique

The calculations were based on the heat conduction equation and were carried out by the matrix method for differential equations. For the function of three spatial variables (x, y, z) and the time variable t, the heat conduction equation is

$$\rho c \frac{\partial T}{\partial t} + \frac{\partial q_x}{\partial x} + \frac{\partial q_y}{\partial y} + \frac{\partial q_z}{\partial z} = 0 , \quad (1)$$

Where ρ is the heat-conducting material's density, c is the specific heat capacity, and q_x, q_i and q_i are the projections of the heat flux density vector

$$q_x = -\lambda \frac{\partial T}{\partial x} , \; q_y = -\lambda \frac{\partial T}{\partial y} , \; q_z = -\lambda \frac{\partial T}{\partial z} \quad (2)$$

Here λ is the thermal conductivity. The specific heat capacity at liquid-helium temperatures is determined by the equation

$$c = \gamma T + AT^3 , \quad (3)$$

Where the coefficient A indicates the contribution of phonons and γ (Somerfield coefficient) presents the contribution of electrons. For simplicity of calculations, the phonon contribution to the heat capacity is not taken into account (A = 0). The operating temperature of the detector was taken to be 9 K, since at this temperature CeB_6 crystals have the highest value of thermoelectric Fig. of merit. The used in calculations parameters are given in Table 1.

Table 1. Parameters of used materials at 9 K [27-30].

Parameters	Material	
	W	CeB_6
Density, kg/m^3	19250	4800
Specific heat capacity, J/kg·K	0.197	7.3
Sommerfeld coefficient, J /kg·K^2	0.022	0.8
Thermal conductivity, W/m·K	9680	1.5
Seebeck coefficient, μV/K	-	150

The thermal processes were modeled according to the following algorithm.

- The entire volume of the absorber and the bridge was broken down into the cells with the dimensions Δx, Δy and $\Delta z \leq 0.1$ μm. Obviously, the enlargement of the number of cells will provide more accurate calculations, but it will lead to more time consuming.

- The initial temperature for the all cells was set 9 K. In the absorber was chosen the cell where the photon is absorbed.

- According to the formula $\Delta T = E / V \cdot \rho \cdot c$, where E is the energy of the absorbed photon and V is the cell volume, the initial temperature of the cell T_0 = 9 K + $+\Delta T$ was calculated.

The temperature of the all cells for each time point it was determined by the equation:

$$T_{ijk}(t_{n+1}) = T_{ijk}(t_n) + \\ + \frac{\Delta t}{\rho c}\left[\frac{\lambda(T_{i+1})+\lambda(T_i)}{2}\cdot\frac{T_{i+1}-T_i}{\Delta x^2} + \frac{\lambda(T_{j+1})+\lambda(T_j)}{2}\cdot\frac{T_{j+1}-T_j}{\Delta y^2} + \frac{\lambda(T_{k+1})+\lambda(T_k)}{2}\cdot\frac{T_{k+1}-T_k}{\Delta z^2}\right] \quad (4)$$

Here i, j, k are the coordinates of the cell, n is the number of time interval from the beginning of the process, Δt is the time interval. Obviously, the value of Δt also determines the accuracy and speed of the calculation.

The absorber thickness is the most important parameter of the TSPD sensor. We were selecting this parameter proceeding from the demand to provide for high probability of photon absorption in the absorber. Taking the Bouguer-Lambert law and using the values for the coefficient of linear attenuation in W for 1 keV, 100 eV and 10 eV energy photons equal to respectively 5.775 μm^{-1}, 28.875 μm^{-1} and 115.5 μm^{-1} [31], it is easy to calculate that the probability of absorption in 1.5 μm thick W of a photon of 1 keV energy will be 0.9998. The absorption probability for 100 eV and 10 eV photons in respectively 0.5 μm and 0.1 μm thick W will exceed 0.9999. It is obvious that thinner tungsten absorbers or absorbers fabricated from not heavy metals can be used to provide for absorption of photons with energies less than 10 eV with the same probability. However, we shall not consider the characteristics of such sensors for the following three reasons. We do not want to enlarge the volume of the article, as well as to complicate its perception. The third reason is that a sensor with 0.1 μm thick tungsten absorber can be successfully used for detection of 1 - 10 eV photons. The obtained results give evidence for that.

Fig. 2 shows the graphs for the probability of reaching by photons of 1 keV, 100 eV and 10 eV energies definite depths in the W absorber and showing that the probability for absorption in upper layers of the absorber is the highest.

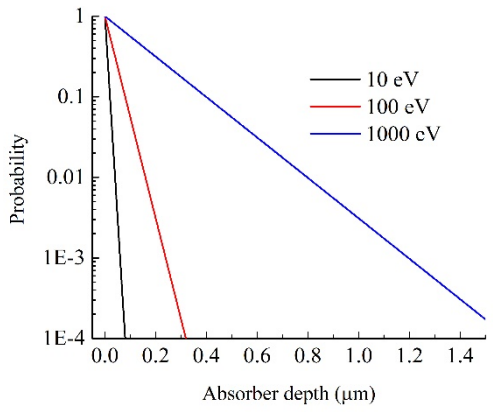

Fig. 2. Probability of reaching by a photon a definite depth in the tungsten absorber.

The calculations for heat propagation processes in the three-layer TSPD sensor are therefore carried out for the cases of photon absorption close to surface of the absorber.

Let us also mention that in the multilayer option of the sensor the heat removal may be provided by using not heavy metal. In the case of necessity, the multilayer sensor versions employing various materials for the heat sink can be considered.

4. Results

The geometrical dimensions of sensors and results of calculations of heat propagation in the three-layer sensor are presented in Table 2.

The columns in the table give the calculation number, the geometric dimensions of absorber (X, Y, Z_1), the thickness of thermoelectric layer (Z_2), the thickness of heat sink (Z_3), the distance from surface of absorber in which photon is absorbed (h), the photon energy (E), the maximum temperature difference on the thermoelectric layer after photon absorption – (ΔT_m), time duration to achieve the ΔT_m – (t_m), the maximum of voltage on the sensor (U_m), the time of recession ΔT to the background 10^{-4} K – (t_b), its inverse (count rate) – (R). In accordance with Fig. 1, the geometric dimensions X and Y of the thermoelectric layer and of the heat sink are similar to those of absorber. In the calculations it was assumed that the photon is thermalized in the center of the absorber surface.

We shall start the discussion of the obtained results with consideration of X-ray photon absorption. Let us investigate the temporal behavior of the temperature difference $\Delta T(t)$ between the two surfaces of the thermoelectric layer in five different parts of the sensor which are at different distances from the sensor center.

The graphs of this dependence for the calculation 1 M from Table 2 are given on Fig. 3. As expected, the highest values for the temperature difference are reached in region 1, i.e. in the center of the sensor, directly under the point of photon thermalization. With distancing from the center the signal weakens and in the point 5 (which is the most far) the maximum is reached in 3 ps from the moment of photon absorption; it is of the order of the background value, 10^{-4} K. A similar result is seen for the rest of calculations, and since the value of arising voltage on the sensor is determined by the maximal temperature difference on the thermoelectric layer, we shall consider further only the dependences $\Delta T(t)$ calculated for region 1.

Note that the graphs shown on Fig. 3 practically merge after 4 ps from the process start. During this time period the heat generated by the photon has already spread throughout the absorber volume.

Table 2. W/CeB_6/W three-layer sensor geometry and calculated parameters.

No	X, Y, Z_1, μm	Z_2, μm	Z_3, μm	h, μm	E, eV	ΔT_m, mK	t_m, ps	U_m, μV	t_b, ps	R, GHz
1M	10, 10, 1.5	1	1	0.1	1000	6.78	0.162	1.017	>10000	<0.1
2M	10, 10, 1.5	0.5	1	0.1	1000	6.78	0.162	1.017	>10000	<0.1
3M	10, 10, 1.5	0.1	1	0.1	1000	6.75	0.156	1.013	420	2.4
4M	10, 10, 1.5	0.05	1	0.1	1000	6.75	0.156	1.013	186.6	5.4
5M	10, 10, 1.5	0.01	1	0.1	1000	5.64	0.156	0.846	4.8	208
6M	10, 10, 1.5	0.01	2	0.1	1000	5.64	0.156	0.846	4.8	208
7M	10, 10, 1.5	0.01	5	0.1	1000	5.64	0.156	0.846	4.8	208
8M	10, 10, 1.5	0.01	1	0.1	1100	6.2	0.156	0.93	5.1	196
9M	10, 10, 1.5	0.01	1	0.1	900	5.07	0.156	0.761	4.5	222
10M	10, 10, 1.5	0.01	1	0.1	1010	5.69	0.156	0.854	4.8	208
11M	20, 20, 1.5	0.01	1	0.1	1000	5.64	0.156	0.846	3.9	256
12M	5, 5, 1.5	0.01	1	0.1	1000	5.64	0.156	0.846	8.7	114
13M	10, 10, 0.5	0.05	1	0.1	100	36.8	0.012	5.52	21.9	45.7
14M	10, 10, 0.5	0.05	1	0.1	110	40.48	0.012	6.072	25.5	39.2
15M	10, 10, 0.5	0.05	1	0.1	90	33.12	0.012	4.968	18	55.5
16M	10, 10, 0.5	0.01	1	0.1	100	33.71	0.012	5.057	2.97	337
17M	10, 10, 0.5	0.01	2	0.1	100	33.71	0.012	5.057	3	333
18M	10, 10, 0.5	0.01	5	0.1	100	33.71	0.012	5.057	3	333
19M	10, 10, 0.1	0.01	1	0.01	10	114.7	0.0015	17.2	1.32	758
20M	10, 10, 0.1	0.01	1	0.01	11	126.1	0.0015	18.9	1.44	694
21M	10, 10, 0.1	0.01	1	0.01	9	103.3	0.0015	15.5	1.2	833
22M	10, 10, 0.1	0.01	1	0.01	7	80.3	0.0015	12.05	0.963	1038
23M	10, 10, 0.1	0.01	1	0.01	4	45.9	0.0015	6.885	0.651	1536
24M	10, 10, 0.1	0.01	1	0.01	1	11.5	0.0015	1.725	0.303	3300
25M	10, 10, 0.1	0.01	1	0.01	1.1	12.6	0.0015	1.89	0.321	3115
26M	10, 10, 0.1	0.01	1	0.01	0.9	10.3	0.0015	1.545	0.282	3546
27M	10, 10, 0.5	0.01	1	0.2	100	71.3	0.0069	10.695	2.1	476
28M	10, 10, 0.5	0.01	1	0.3	100	179.7	0.004	26.955	2.1	476
29M	10, 10, 1	0.01	1	0.1	100	3.4	0.06	0.51	1.671	598
30M	10, 10, 1	0.01	1	0.2	100	4.0	0.045	0.6	1.659	602
31M	10, 10, 1	0.01	1	0.3	100	5.6	0.033	0.84	1.644	608
32M	10, 10, 0.5	0.01	0.5	0.1	100	33.7	0.012	5.057	2.85	351
33M	10, 10, 0.5	0.01	0.1	0.1	100	33.7	0.012	5.057	2.191	456
34M	10, 10, 0.5	0.01	0.05	0.1	100	33.7	0.012	5.057	1.699	589
35M	10, 10, 0.1	0.01	0.5	0.01	1	11.5	0.0015	1.722	0.30561	3272
36M	10, 10, 0.1	0.01	0.1	0.01	1	11.5	0.0015	1.722	0.30705	3257
37M	10, 10, 0.1	0.01	0.05	0.01	1	11.5	0.0015	1.722	0.30711	3256

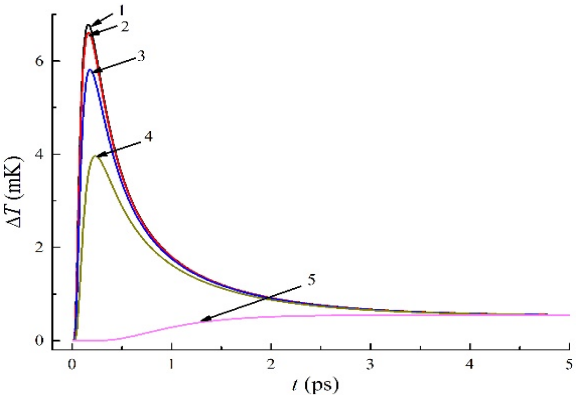

Fig. 3. $\Delta T(t)$ dependence of the calculation 1M measured in five different areas of the thermoelectric layer: in the center (1), at different distances from the center: 0.2 μm (2), 0.5 μm (3), 1 μm (4), 5 μm (5).

After that, the heat must pass through the thermoelectric layer.

It follows from the table data that for the calculation 1M decay time to the background level is above 10 ns. The reason for this is in the low value of thermal conductivity coefficient of CeB_6. Acceleration of the heat transfer from absorber to the heat sink can be achieved by decreasing the thickness of the thermoelectric layer. In calculations 1 M – 5 M, the thermoelectric latter was gradually decreased from 1 μm to 0.01 μm. The graphs of $\Delta T(Z_2)$ and $t_b(Z_2)$ dependencies of these calculations are presented on Fig. 4.

We can see that parameter t_b is decreasing upon decreasing of the thickness of the thermoelectric layer, while the values of the parameter ΔT_m remain practically unchanged up to 0.05 μm thicknesses. Parameter ΔT_m is somewhat smaller for the 0.01 μm thick thermoelectric layer but at the same time the

signal is going down to the background value much faster thus providing for counting rate of the order of 200 GHz. In further calculations we shall use this value for the thickness of the thermoelectric layer.

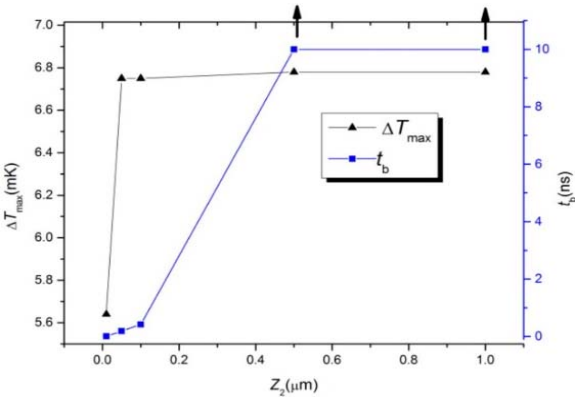

Fig. 4. Dependence of the ΔT_m and t_b parameters of calculations 1 M – 5 M on the thickness of the thermoelectric layer.

Let compare the results of calculations 5-7 for sensors with 1-5 μm thicknesses of the W heat sink. It is seen from Table 2 that variation of the heat sink thickness does not influence the value of maximum signal and the count rate. It can be concluded that the thickness of the heat sink does not have a significant influence on the characteristics of the sensor and can be selected taking into account other constructional demands.

Fig. 5 shows $\Delta T(t)$ graphs for the cases of 1 keV and 1 ± 0.1 keV photon absorption. It can be seen that change of photon energy leads to change in the ΔT_m value, while t_m does not change. It follows from Table 2 that the U_m values differ by 85 nV, if the photon energies differ by 10 %, and by 8 nV, if they differ by 1 %. It should be also mentioned that change in photon energy leads to some change of the count rate. Parameter R is smaller in the case of higher photon energies, since after thermalization in the absorber of the photon with a higher energy the temperature difference resulting on the thermoelectric layer is going down slower to the background value.

The next calculations in Table 2 are performed for sensors having twice larger dimensions on X and Y coordinates (11 M) and twice smaller dimensions (12 M). Comparison of their characteristics with those for calculation number 5 M shows that in the first case the count rate increases from 208 GHz to 256 GHz, while in the second case it decreases down to 114 GHz. Their ΔT_m values in the meantime do not differ. From comparison of these data with those graphs of Fig. 3 it can be stated that in a three-layer sensor the TSPD absorber carries out not only the task of transformation of the photon energy to heat, but also of heat transfer from the thermalization zone of the photon. It is evident that these fact favors a remarkable increase of the count rate.

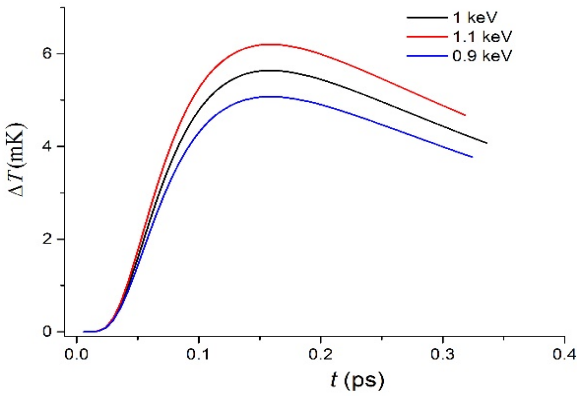

Fig. 5. $\Delta T(t)$ dependencies of calculation numbers 5 M, 8 M, 9 M for the cases of absorption of photons with 1000 eV, 1100 eV and 900 eV energies.

Now let us consider the calculations on detection of UV photons with energies above 100 eV, which border with X-ray energies, to 4 eV, or to the border of the visible range. Absorption of photons in calculations 13 M – 15 M is considered with energies of 100 eV and 100 ± 10 eV in 0.5 μm thick tungsten absorber. It follows from Table 2 that the voltages corresponding to maximums of these dependences differ by 0.55 μV. Registration of signals differing by nanovolts will prove achievement of 0.1 eV energy resolution.

Comparison of ΔT_m parameters for 4 M and 13 M calculations shows that as a result of a 100 eV photon absorption this parameter is bigger almost by one order, than in the case of X-ray photons. Explanation of this fact will be given later. Now we shall consider the results of 16 M – 18 M calculations which have been carried out for the sensor geometries with different thicknesses of the tungsten heat sink and the thermoelectrics thickness of 0.01 μm. In this case, as it follows from the table, the thickness of the heat sink does not influence the parameters ΔT_m, t_m, U_m, t_b and R. However, in comparison to the previous 3 calculations, when the thickness of the thermoelectric layer was 0.05 μm, the count rate is remarkably higher. It goes up to 333 GHz that exceeds the known to us literature values for this parameter in superconducting detectors.

Calculations presented in Table 2 for 11 eV and smaller photon energies were done for the sensor with 0.1 μm absorber thickness. As mentioned above, such a thickness of the W absorber provides for photon absorption in the given energy range with probability close to 1. Calculations 19 M – 21 M were carried out for the case of photon absorption with energy 10 eV and 10 ± 1 eV. Parameter ΔT_m for these calculations is also much bigger, as compared to the value of this parameter in calculations 8 M – 10 M, although the photon energy is decreased by one order. This seems strange, as in the above case, when comparing the calculation results for the cases of 1 keV and 100 eV photons absorption. The situation is cleared if taking into account the change of the absorber thickness. When going from X-ray photons to UV photons with

100 eV energy we had decreased the absorber thickness Z_1 from 1.5 μm to 0.5 μm, or by a factor of 3, and correspondingly by a factor of 5, up to 0.1 μm upon changing the photon energy from 100 eV to 10 eV. Calculations of ΔT to which the tungsten semi-sphere will be heated by a photon of energy E give for the 3 considered cases the following values: E = 1 keV, Z_1 = 1.5 μm, ΔT = 0.008 K; E = 100 eV, Z_1 = 0.5 μm, ΔT = 0.022 K; E = 10 eV, Z_1 = 0.1 μm, ΔT = 0.352 K. These values of ΔT correspond to the values of ΔT_m in calculations 5 M, 16 M and 19 M.

From the data of Table 2 for absorption of photons of 10 eV, 11 eV and 9 eV energies, the values of the U_m parameter are equal correspondingly to 17.2 μV, 18.9 μV and 15.5 μV. The 1 eV difference in energy, at the level of 10 eV, corresponds to the voltage of 1.7 μV, or the registration of the signal with 0.17 μV accuracy will provide for a 0.1 eV energy resolution. At the same time it is a pleasure to state that parameter R of calculations 19 M – 21 M constitutes a few hundreds of gigahertz.

Dependence of the U_m parameter on energy of the absorbed photon for calculations 19 M – 26 M is presented on Fig. 6. These calculations were carried out at similar geometric sizes of the sensor layers. The observed in this case linearity shows that the U_m parameter, or the measured in the experiment maximum of arising voltage on the sensor, can be used for exact determination of the energy of the absorbed photon.

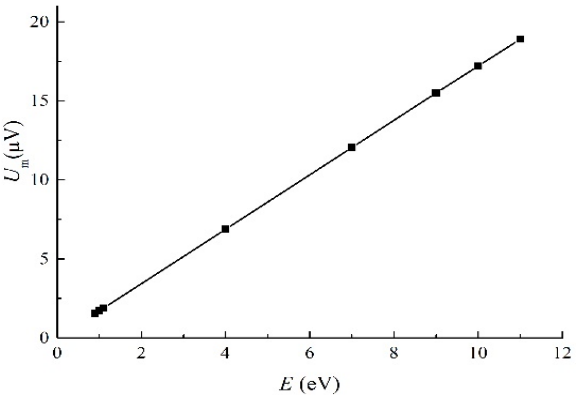

Fig. 6. Dependence of the U_m parameter from calculations 19M – 26M on the energy of absorbed photon.

According to data of Table 2, for IR photons with energies of 0.9 eV, 1 eV and 1.1 eV (calculations 24 M – 26 M) the U_m parameter is equal respectively to 1.545 μV, 1.725 μV and 1.89 μV. Thus, the 0.1 eV energy difference at 1 eV level corresponds to U_m parameter difference by 0.18 μV. It can be stated, that for the IR photons the accuracy of the photon energy valuation can also be better than 1 %.

Let us pay attention to the count rate parameter for the calculations 22 M – 26 M given in Table 2. The data show that for the near UV range, as well as for the IR, the photon count rate may reach terahertz values. The count rate of the single layer sensor of TSPD, as well as of superconducting detectors, is by orders of magnitude lower [20-23].

Let us consider the case, when the photon is absorbed at some distance below the absorber surface. As it has been shown above (Fig. 2) the probability for a photon to reach a certain depth in the absorber is strongly reduced with increasing this depth. Nevertheless, we have done calculations for processes of heat distribution in a three-layer sensor of TSPD upon absorption of a 100 eV energy photon at different depths from the absorber surface. At the same dimensions of the sensor, calculations 4 M, 27 M and 28 M were done for the cases of photon absorption at 0.1 μm, 0.2 μm and 0.3 μm distances from 0.5 μm thick absorber surfaces. Fig. 7 shows $\Delta T(t)$ graphs for these calculations. Calculations 29 M, 30 M and 31 M were done for photon absorption at the same depths, but in a 1 μm thick absorber. As it can be seen from Fig. 7 the signal, as expected, is amplified and the maximum is reached faster when the point of photon thermalization is approaching the thermoelectric layer. Similar results are obtained for calculations 29 M – 31 M (see Table 2). With increasing h, higher values of parameter ΔT_m are reached, while parameter t_m is decreasing.

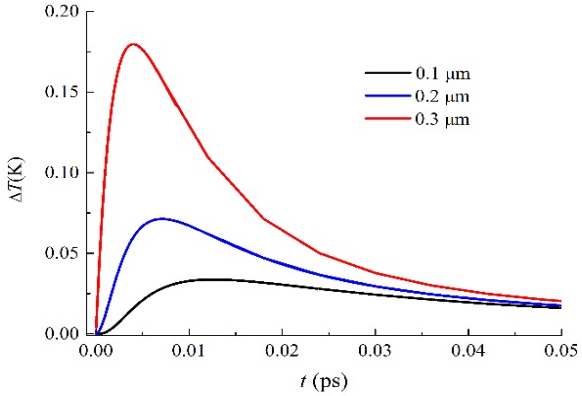

Fig. 7. $\Delta T(t)$ dependencies of calculation numbers 4 M, 27 M, 28 M for the cases of absorption of photons with 100 eV energy at 0.1 μm, 0.2 μm and 0.3 μm distances from absorber surface.

Analysis of data of Table 2 allows concluding that, at the same architecture of the sensor, parameter t_m depends on the distance from absorber surface at which photon is absorbed (h), while t_m and ΔT_m parameters uniquely define the energy of the absorbed photon.

Finally, let us consider sensors with the heat sink thinner than 1 μm. The characteristics of sensors with a thin heat sink may differ from the results of previous calculations. The need for such sensors may arise for solution of some specific tasks. The thickness of the heat sink in calculations 1 M – 31 M was varied in the range 1 - 5 μm, and we came to the conclusion that such a change of the heat sink thickness did not change the characteristics of the signal obtained after photons

absorption. Calculations 32 M – 37 M reveal that the t_m and ΔT_m signal parameters do not change when the thickness of the heat sink becomes less than 1 μm. Parameters t_b, and therefore the count rate are changing. Moreover, as it follows from the data given in Table 2, this change is different for photons of different energies. Fig. 8 clearly shows that with decreasing of the heat sink thickness, parameter R increases for calculations describing the absorption of photons with 100 eV energy, while it decreases in the case of absorption of 1 eV photons. This strongly different behavior becomes understandable after a more detailed consideration of processes of heat propagation in a three-layer sensor.

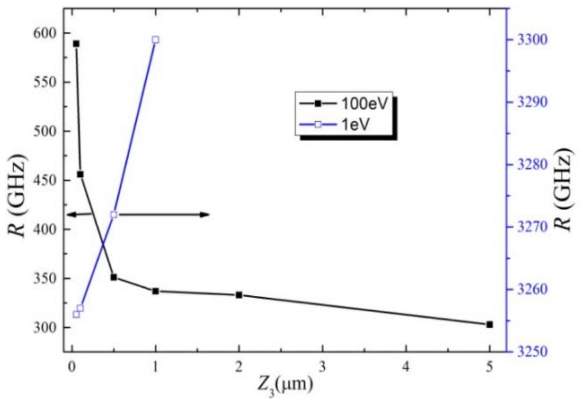

Fig. 8. Dependence of parameter R from calculations for 1eV and 100 eV energy photons on the thickness of heat sink.

Let us check how is changing with time the temperature at the thermoelectric-heat sink boundary (T_1) directly under the zone of photon thermalization. Fig. 9 shows $T_1(t)$ graphs for the cases of 1 eV (calculation 37 M) and 100 eV (calculation 34 M) photon absorption in the sensor with a 50 nm thick heat sink for time interval $0 – t_b$.

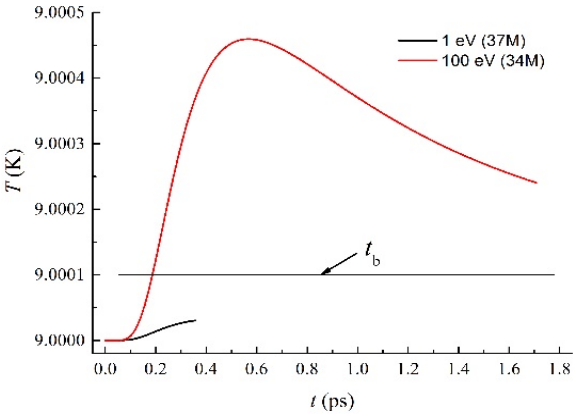

Fig. 9. $T_1(t)$ dependence for 1 eV and 100 eV photons absorbtions in the sensors with heat sink of 50 nm thickness.

As seen, these graphs largely differ. While upon absorption of 100 eV photons this zone is heated to T_1 which is exceeding by 4 times the background temperature (T_b), in the case of 1 eV photon absorption the value of T_1 is significantly lower than T_b. At the same time we see different dynamics of heat propagation processes for the two calculations which is the reason for the differences shown in Fig. 8.

Note that the changes of parameter R versus the thickness of the heat sink is small. According to calculations, for 100 eV photons the decrease in thickness of the heat sink by a factor of 100 leads to increase of the parameter R by less than two times; for the case of 1 eV photons the decrease in thickness of the heat sink by a factor of 20 leads to reduction of the parameter R by 1.3 %.

Is it realistic to measure the signal from the thermoelectric sensor considered in the present work?

1) The following results or data were considered in previous papers [11, 16] concerning the principal possibility of conversion of the thermoelectric energy to electrical voltage and digital superconducting readout:

- Experimental registration of the signal coming from thermoelectric single layer sensor consisting of Sb absorber and heat-sink with an Au-Fe thermoelectric bridge between them;
- Signal acquisition scheme in single-pixel experiments.

Thermoelectric sensors can function as either voltage or current sources. The low working temperatures and low impedance of the sensors facilitate using SQUIDs as preamps for the lowest noise. SQUIDs measure current and transform it into voltage. Three important conclusions on the signal registration chain are apparent from this scheme:

a) Any parasitic resistance should be eliminated (in devices, interconnections, etc.).

b) Input/output impedances should match in cold stage (detector unit and superconductor electronics), and in room temperature stage, the amplifier input noise should be lower than the output noise level from the SQUID preamplifier.

c) Signal acquisition bandwidth should be optimized.

Concluding this part, we can state that the signal of the thermoelectric detector operating at helium temperatures can be registered.

2) As it is shown in the present work, the voltage appearing on the sensor can reach micro-volts; to provide an energy resolution of better than 1 %, it is necessary to have resolution of a few nanovolts. Registration of such a signal of sensor of TSPD can be realized without difficulties for signal of nanosecond durations [11].

3) For shorter duration signals the approaches commonly used in superconducting detectors can be used in registration of the signal of the thermoelectric sensor, since despite of very different physical processes underlying these two types of detectors, the final stage is the registration of the out-coming electrical signal, while electronics is indifferent to the

origin of the signal and as a result of which physical processes it is originating.

In conclusion, summing these arguments we can give a positive answer to the above raised question on possibility of signal registration coming from the thermoelectric sensor considered in this work.

5. Conclusions

The obtained results allow the following conclusions to be done:

1) The three-layer sensor of TSPD may register individual photons in a wide range of the electromagnetic spectrum from 1 eV to 1 keV, providing energy resolution of not less than 1 % and count rate from tens gigahertz to terahertz.

2) For solution of a wide range of different tasks the ratio (energy resolution)/(count rate) can be varied by changing the geometric sizes of the sensor.

3) Taking into account several features of the thermoelectric detector, such as simple design, high position resolution and absence of strict requirements to operating conditions, it can be argued that thermoelectric detectors with multi-layer sensor can be a real competitor to superconducting detectors.

The superconducting single photon detectors have a longer history of development, as compared to thermoelectric ones. A big number of research groups have been involved and continue the studies on superconducting detectors at present in many countries that resulted in remarkable improvement of SSPD characteristics. The authors hope that the present publication will attract attention to thermoelectric detectors and that the experimental results on TSPD research will appear soon, since following the results of computer simulation this is quite a perspective direction.

Acknowledgements

This work was supported by the RA MES State Committee of Science and Russian Foundation for Basic Research (RF) in the frames of the joint research projects SCS 15RF-018 and RFBR 15-53-05047 accordingly.

The authors would like to thank Dr. A.M. Gulian for the helpful discussions.

References

[1]. R. H. Hadfield, Single-photon detectors for optical quantum information applications, *Nature Photonics,* Vol. 3**,** No. 12, 2009, pp. 696-705.

[2]. J. J. Renema, Q. Wang, R. Gaudio, I. Komen, K. Hoog Op'T, D. Sahin, A. Schilling, M. P. van Exter, A. Fiore, A. Engel, M. J. A. de Dood, Position-Dependent Local Detection Efficiency in a Nanowire Superconducting Single-Photon Detector, *Nano Letters,* Vol. 15, No. 7**,** 2015, pp. 4541-4545.

[3]. M. Kaniber, F. Flassig, G. Reithmaier, R. Gross, J. J. Finley, Integrated superconducting detectors on semiconductors for quantum optics applications, *Applied Physics B,* Vol. 122, No. 115, 2016, pp. 1-2.

[4]. T. Yamashita, S. Miki, H. Terai, Z. Wang, Low-filling-factor superconducting single photon detector with high system detection efficiency, *Optics Express*, Vol. 21, Issue 22, 2013, pp. 27177-27184.

[5]. K. D. Irwin, Seeing with Superconductors, *Scientific American,* Vol. 295, 2006, pp. 86-95.

[6]. J. N. Ullom, D. A. Bennett, Review of superconducting transition-edge sensors for X-ray and gamma-ray spectroscopy, *Superconductor Science and Technology,* Vol. 28, No. 8, 2015, 084003.

[7]. G. N. Gol'tsman, O. Okunev, G. Chulkova, A. Lipatov, A. Semenov, K. Smirnov, B. Voronov, A. Dzardanov, C. Williams, R. Sobolewski, Picosecond superconducting single-photon optical detector, *Applied Physics Letters*, Vol. 79, No. 6, 2001, pp. 705-707.

[8]. H. A. Atikian, A. Eftekharian, J. A. Salim, M. J. Burek, J. T. Choy, H. A. Majedi, M. Lončar, Superconducting nanowire single photon detector on diamond, *Applied Physics Letters*, Vol. 104, Issue 12, 2014, 122602.

[9]. D. Liu, S. Miki, T. Yamashita, L. You, Z. Wang, H. Terai, Multimode fiber-coupled superconducting nanowire single-photon detector with 70 % system efficiency at visible wavelength, *Optics Express,* Vol. 22, Issue 18, 2014, pp. 21167-21174.

[10]. J. J. Renema, R. Gaudio, Q. Wang, Z. Zhou, A. Gaggero, F. Mattioli, R. Leoni, D. Sahin, M. J. A. de Dood, A. Fiore, M. P. van Exter, Experimental test of theories of the detection mechanism in a nanowire superconducting single photon detector, *Phys. Rev. Lett.*, Vol. 112, No. 11, 2014, 117604.

[11]. G. G. Fritz, K. S. Wood, D. van Vechten, A. L. Gyulamiryan, A. S. Kuzanyan, N. J. Giordano, T. M. Jacobs, H**.-**D**.** Wu, J. S. Horwitz, A. M. Gulian, Thermoelectric single-photon detectors for X-ray/UV radiation, *Proc. SPIE*, Vol. 4140, 2000, pp. 459-469.

[12]. D. Van Vechten, K. Wood, G. Fritz, J. Horwitz, A. Gyulamiryan, A. Kuzanyan, V. Vartanyan, A. Gulian, Imaging detectors based on anisotropic thermoelectricity, *Nuclear Instruments and Methods in Physics Research*, Vol. 444, Issue 1-2, 2000, pp. 42-45.

[13]. S. N. Song, S. R. Maglic, C. D. Thomas, M. P. Ulmer, J. B. Ketterson, High energy resolution X-ray detection based on a coupled Fiske cavity and Josephson junction oscillator, *Applied Physics Letters*, Vol. 69, No. 11, 1996, pp. 1631-1633.

[14]. K. Wood, D. Van Vechten, G. Fritz, H.-D. Wu, S. Bounnak, K. Bussman, K. Winzer, S. Kunii, V. Gurin, M. Korsukova, C. Mitterer, M. Corlsson, F. Golf, A. Kuzanyan, G. Badalyan, S. Horutyunyan, S. Petrosyan, V. Vardanyan, T. Paronyan, V. Nikoghosyan, A. Gulian, Toward Ultimate Limits of Performance of the QVD Detector, *Nuclear Instruments and Methods in Physics Research*, Vol. 520, Issue 1-3, 2004, pp. 56-59.

[15]. A. Gulian, K. Wood, D. VanVechten, G. Fritz, H.-D. Wu, S. Bounnak, K. Bussman, K. Winzer, S. Kunii, V. Gurin, M. Korsukova, C. Mitterer, M. Corlsson, F. Golf, A. Kuzanyan, G. Badalyan, S. Horutyunyan, S. Petrosyan, V. Vardanyan, T. Paronyan, V. Nikoghosyan, Current developmental status of thermoelectric (QVD) detectors, *Nuclear Instruments*

and Methods in Physics Research, Vol. 520, Issue 1-3, 2004, pp. 36-40.
[16]. A. Gulian, K. Wood, D. Van Vechten, G. Fritzdet, Cryogenic thermoelectric (QVD) detectors: Emerging technique for fast single-photon counting and non-dispersive energy characterization, *Journal of Modern Optics*, Vol. 51, Issue 9-10, 2004, pp. 1467-1490.
[17]. V. A. Petrosyan, Hexaborides of Rare Earths as a Sensor Material for Thermoelectric Single-Photon Detectors, J. *Contemp. Phys. (Arm. Acad. Sci.)*, Vol. 46, 2011, pp. 125-128.
[18]. A. A. Kuzanyan, V. A. Petrosyan, A. S. Kuzanyan, Thermoelectric single-photon detector, *Journal of Physics: Conference Series*, Vol. 350, No. 1, 2012, 012028.
[19]. A. A. Kuzanyan, A. S. Kuzanyan, Thermoelectric Nanowire Single-Photon Detector, *Proc. of SPIE*, Vol. 8773, 2013, 87730L-1.
[20]. A. A. Kuzanyan, Nanosensor for Thermoelectric Single-Photon Detector, *Nano Studies*, Vol. 9, 2014, pp. 93-102.
[21]. A. Kuzanyan, V. Nikoghosyan, A. Kuzanyan, Modeling of Kinetic Processes in Thermoelectric Single Photon Detectors, *Proc. of SPIE*, Vol. 9504, 2015, 95040O.
[22]. A. Kuzanian, V. Nikoghosyan, A. Kuzanyan, CeB_6 Sensor for Thermoelectric Single-Photon Detector, *Sensors & Transducers*, Vol. 191, Issue 8, August 2015, pp. 57-62.
[23]. A. A. Kuzanyan, A. S. Kuzanyan, V. R. Nikoghosyan, Ultrafast TSPD on the basis of CeB_6 sensor, *Journal of Physics: Conference Series*, Vol. 673, 2016, p. 012007.
[24]. A. Kuzanyan, A. Kuzanyan, V. Nikoghosyan, Multi-layer sensor of thermoelectric detector, Patent of Armenia № 2946, 2015.
[25]. A. A. Kuzanyan, A. S. Kuzanyan, V. R. Nikoghosyan, V. N. Gurin, M. P. Volkov, Investigation of processes of heat propagation in multilayer sensor of thermoelectric single-photon detector, *Journal of Contemporary Physics (Arm. Acad. Sci.)*, Vol. 51, Issue 2, 2016, pp. 181-190.
[26]. K. S. Wood, G. G. Fritz, A. M. Gulian, D. Van Vechten, Photon detector, *US Patent US 6,710,343* B2, 2004.
[27]. V. Petrosyan, V. Vardanyan, V. Kuzanyan, M. Konovalov, V. Gurin, A. Kuzanyan, Thermoelectric properties and chemical composition of CeB_6 crystals obtained by various methods, *Solid State Sciences*, Vol. 14, Issue 11-12, 2012, pp. 1653-1655.
[28]. T. R. Waite, R. S. Craig, W. E. Wallace, Heat Capacity of Tungsten between 4 and 15°K, *Phys. Rev. Lett.*, Vol. 104, Issue 5, 1956, pp. 1240-1241.
[29]. S. R. Harutyunyan, V. H. Vardanyan, A. S. Kuzanyan, V. R. Nikoghosyan, S. Kunii, K. S. Wood, A. M. Gulian, Thermoelectric cooling at cryogenic temperatures, *Applied Physics Letters*, Vol. 83, Issue 11, 2003, pp. 2142-2144.
[30]. Y. Peysson, C. Ayache, B. Salce, J. Rossat–Mignod, S. Kunii, T. Kasuya, Thermal conductivity of CeB_6 and LaB_6, *Journal of Magnetism and Magnetic Materials*, Vol. 59, 1986, pp. 33-40.
[31]. C. T. Chantler, Theoretical Form Factor, Attenuation and Scattering Tabulation for Z=1-92 from E=1-10 eV to E=0.4-1.0 MeV, *Journal of Physical and Chemical Reference Data,* Vol. 24, Issue 1, 1995, pp. 71-643.
